

We are IntechOpen, the world's leading publisher of Open Access books Built by scientists, for scientists

6,900

Open access books available

185,000

International authors and editors

200M

Downloads

Our authors are among the

154

Countries delivered to

TOP 1%

most cited scientists

12.2%

Contributors from top 500 universities



WEB OF SCIENCE™

Selection of our books indexed in the Book Citation Index
in Web of Science™ Core Collection (BKCI)

Interested in publishing with us?
Contact book.department@intechopen.com

Numbers displayed above are based on latest data collected.
For more information visit www.intechopen.com



Coastal Altimetry: A Promising Technology for the Coastal Oceanography Community

Xi-Yu Xu, Ke Xu, Ying Xu and Ling-Wei Shi

Abstract

Satellite altimetry has been one of the most important implements for physical oceanographers. The conventional altimeter is best performed over open ocean surface, yet there are many attempts to exploit the potential of altimetry in coastal zone in the last decade. To achieve a high performance for coastal altimetry is a multi-fold effort: the more sophisticated instrument concepts, the smarter onboard trackers, the more expert data editing criteria, the more specific retracking algorithms, the more advanced error correction methods, etc. In this chapter, each of the above aspects is described in detail, and some representative works in the altimetry community are reviewed. Particularly, the coastal altimetry offshore Hong Kong is addressed as a case study to demonstrate the potential of the new technology. In the conclusive session, some prospects for the coastal oceanography community are presented.

Keywords: coastal zone, altimetry, retracker, error correction, Hong Kong

1. Introduction

Coastal altimetry has been one of the key remote sensing technologies in the coastal zone where the effects of a changing climate are most severely felt. For over a quarter century, satellite altimetry technology has been used to routinely monitor sea level changes over the global open ocean, but was largely unexploited in the coastal areas. Indeed, satellite altimetry was originally designed to precisely measure the sea level of the open ocean, yet it has drawn much attention from the coastal community over the past decade.

This chapter addresses the improvements of this intriguing technology. In Section 2, the principles of satellite altimetry and the recent advances of coastal altimetry technology are reviewed, highlighting the coastal-oriental altimetry products which might attract the attention of the coastal oceanographers. In Section 3, a case study is presented at Hong Kong coast to demonstrate the potential of the new technology. This chapter ends with a brief conclusive and prospective section.

2. A brief review of the advances in coastal altimetry

Coastal altimetry has come on to the central stage of the altimetry community. Coastal altimetry workshops (CAWs) are regularly organized (once every 1 or 2

years) for peers to present their recent researches. A book entitled “Coastal Altimetry” was published in 2011 [1], and significant improvements have been made since then. This section attempts to review some important advances in this field.

2.1 Principles of satellite altimetry

“Coastal altimetry” might be much more familiar for the altimetry community than for the coastal community. A very brief background introduction of satellite altimetry would be presented here, and interested readers are encouraged to refer to the elaborate books such as [2, 3].

The concept of the satellite altimetry is straightforward. A nadir-pointing spaceborne radar transmits short pulses and receives the echoes from the earth (usually, sea) surface. The sea level parameters (range between the satellite and sea surface, significant wave height, and backscatter coefficient) are extracted from the echoes via a process called “retracking”. The altimetric range can be extremely precisely measured in this way. Meanwhile, the satellite orbit can also be precisely determined. After carefully compensating for a variety of error sources, the surface height relative to an absolute datum (usually the reference ellipsoid) can be accurately retrieved, within no more than few centimeters over open ocean surface.

While the satellite altimetry can be dated back to the 1960s [4], one must admit that the Topex-Poseidon satellite launched in 1992 is a benchmark [5]. Thanks to its unprecedented accuracy, it remolded the knowledge scene of many fields in oceanography, such as ocean circulation, ocean tide, El-Nino, and global climate change. Its successors, Jason series satellites, have been extending the high-quality sea level record incessantly [6–8]. Space agencies of Europe, China, and India are also handling altimetry missions, such as ERS-1, ERS-2, Envisat, Saral, and HY-2 [9–12]. Now a constellation of complementary altimetry satellites (with different orbit sampling strategy) have been formed and abundant data are worthy of exploiting. Nowadays, altimetry is not only a fundamental tool for oceanographers and geodesists, but also an attracting resource for those who research into the fields of coastal zone, Cryosphere and inland waters, etc.

2.2 Difficulties in coastal altimetry

Coastal altimetry is not an easy task. There are a couple of difficulties when extending altimetry technology to coastal zone. Firstly, in the coastal band a few kilometers wide (comparable to the altimeter footprint size), radar echoes are severely contaminated by the nearby land surface, leading to complex waveforms significantly departing from that of open ocean. Things are further complicated by the fact that the geographic and environmental characteristics of the coast (e.g., coastline direction, relief, bathymetry, and rain rate) are extremely diverse throughout the world, and altimetric mission (orbit configuration, on-board tracker, flight direction, etc.) are also different. **Figure 1** shows two examples of waveforms, one over the open ocean (a) and the other over a coastal zone (b). Therefore, a specific process called ‘retracking’ is widely employed to extract the sea level parameters from these nonstandard waveforms.

Another difficulty is related to the various corrections applied to the altimeter measurements that are usually less accurate at the coast. The most suffered corrections are wet tropospheric delay, ocean tide correction, dynamic atmospheric correction (DAC), and sea state bias. Consequently, most altimeter data near land are flagged as invalid and eliminated from the standard products.

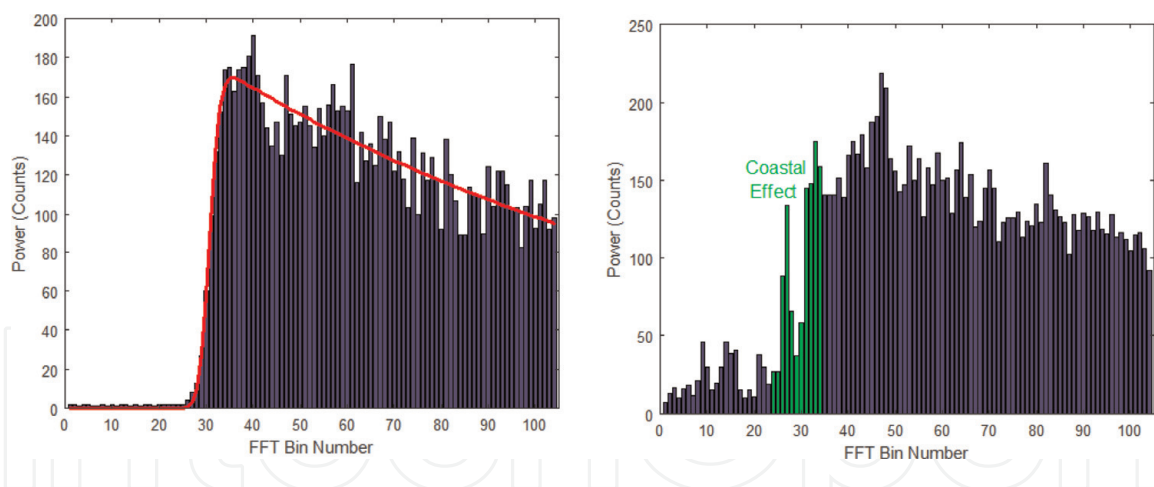


Figure 1.
 Examples of typical open ocean waveform (left, the red line corresponds to the fitted Brown model) and coastal ocean waveform (right).

2.3 Review of the current coastal altimetry products

For about a decade, many efforts have been paid by the altimetry community to overcome the above difficulties and exploit altimetry information near the coast. A number of coastal altimetry products were distributed to the community. For the Jason-2 altimeter, the most popular products are (1) X-TRACK developed by LEGOS (Laboratoire d'Etudes en Géophysique et Océanographie Spatiales, France), (2) PISTACH (Prototype Innovant de Système de Traitement pour l'Altimétrie Côtière et l'Hydrologie, Mercier et al. [15]) developed by CLS (Collecte Localisation Satellites, France), and (3) ALES (Adaptive Leading Edge Sub-waveform, Passaro et al. [14]) developed by NOC (National Oceanography Centre, UK). PEACHI (the Prototype for Expertise on Altimetry for Coastal, Hydrology and Ice, PEACHI) is a sister product of PISTACH while it currently focuses on the Saral/Altika. Corresponding coastal altimetry products are based on dedicated analysis of the nonstandard waveforms and/or sophisticated coastal geophysical corrections [13–15].

X-TRACK is a relatively concise product but does not apply waveform retracking, while ALES and PISTACH are extended products to SGDR (Sensor Geophysical Data Record which includes the waveform distributed by AVISO officially), applying waveform retracking, conserving the official SGDR terms, and annexing new parameters (retracking results and geophysical corrections). ALES does not provide improved geophysical correction, while PISTACH provides 2–3 candidate solutions for almost every geophysical correction term.

X-TRACK is a level 3 (L3) product: using the GDR data and state-of-the-art altimetry corrections, along-track sea level time series projected onto reference tracks (points at same locations for every cycle) are computed at 1-Hz (~6 km along-track resolution). It is simple to use and is based on improved geophysical corrections near the coast (see [6] for details), but its current version only includes the Jason-2 official retracker dedicated to open ocean conditions.

For the geophysical corrections, the advantages of X-TRACK are (1) a more robust median-based editing criterion for the ionosphere correction. (2) A Loess filter (locally weighted scatter plot smoother using a quadratic polynomial model) for the sea state bias correction. (3) A new set of tide solution based on empirical harmonic analysis of the altimetry data.

PISTACH outperforms its counterparts in waveform classification and wet troposphere correction. The decontaminated wet troposphere correction approach is based on the corrected brightness temperature of the on-board radiometer. Another

improvement of PISTACH may be the dedicated sea state bias correction algorithm at the coast, albeit not very reliable due to limited dataset.

ALES simply focuses on the design of an adaptive retracker that can be applied to a variety of waveforms and reduces inconsistency derived from the bias among different retrackers.

The schemes of the three main state-of-the-art coastal altimetry products for Jason-2 satellite altimeter are tabulated in **Table 1**.

2.4 Altimeter waveform processing

The essential part of the altimetry processing is the so-called “waveform retracking”. “Waveform”, as shown in **Figure 1**, records the amplitude of the earth surface echo as a function of time delay. Due to the difference of contexts or traditions, the x-axis of a waveform can be time, frequency, or range, but the three items above can be transformed to each other by simple scaling factors. “Retracking” is the process of extracting useful parameters (range, amplitude, and sometimes significant wave height) from the waveform. The coastal waveforms show very diverse pattern, and it is impractical to find a unique retracker that performs best for every waveform, so it is necessary to classify the waveforms before retracking.

2.4.1 Waveform classification

The classification methodology either relies on statistical characteristic analysis, or on machine learning skills such as neural network. One of the earliest works on

Product	X-TRACK	ALES	PISTACH
Affiliation	LEGOS-CTOH	NOC (UK)	CLS
Reference	Birol et al. [13]	Passaro et al. [14]	Mercier et al. [15]
Style	Concise	Similar to SGDR (CGDR)	Similar to SGDR (IPC)
Coastline model	GSHHS & R. P. Stumpf	GSHHS	GSHHS
Waveform classification	NO	NO	16 classes
Land cover	NO	NO	GLOBCOVER (but seems all with default value)
Waveform retracking	NO	ALES Algorithm	ICE1 + ICE3 + OCE3 + RED3
Ocean tide	FES12 + 73 empirical harmonic constants	=GDR	GDR + GOT 4.7
Wet troposphere	composite correction (ECMWF)	=GDR	composite correction or decontaminated correction
Sea state bias	Loess filtering + missed data interpolating	=GDR	=GDR or New OCE3 model
Geoid	NO	No	GDR + EGM2008
Mean sea surface	MSS CLS01V1	DTU10	GDR + GOCINA
Mean topography	CLS09 (be updated soon)	No	Rio 05 + Rio07 over MedSea
Bathymetry	NO	No	DTM2000.1 + WebTide, Etopo2v2

Table 1.
Review of the three main coastal altimetry products for Jason-2 satellite altimeter [13–15].

waveform classification was carried out by Berry et al. [16]. They set up an expertise system to classify the ERS-1 geodetic mission waveforms over ocean, coast, ice, desert, forest, and land. Their interests lied in the land and forest and their objective was to set up a digital elevation model (DEM) with accuracy from one meter (over plain or desert) to several meters (over plateau).

The official Envisat altimeter ground segment classifies the waveform into four types: ocean, ice sheet, glacier, and sea ice. There is no coastal-oriented retracker, but coastal waveforms are regarded as certain ice types. PISTACH product classifies the waveform into 16 classes, including a “doubt” class (see **Figure 2**). For each class, a certain retracker is assigned [15].

Maybe the most complex classification strategy is the one carried out by Schwatek et al. [17]. They classified the waveform into more than 50 classes. Even over the open ocean they have a dozen of classes. It may be somewhat unnecessarily complicated. Anyway, waveform classification and retracking should be a complete suite of solution for waveform processing.

2.4.2 Waveform retracking

The current waveform retrackers can be split into two groups: the model-based ones and model-free ones.

2.4.2.1 Model-based retrackers

In model-based retrackers, the parameters of interest (range between satellite and sea surface, significant wave height, and backscatter coefficient) are estimated by fitting the waveform to a certain model via a maximum likelihood estimation (MLE) approach. What really counts is the choice of the model.

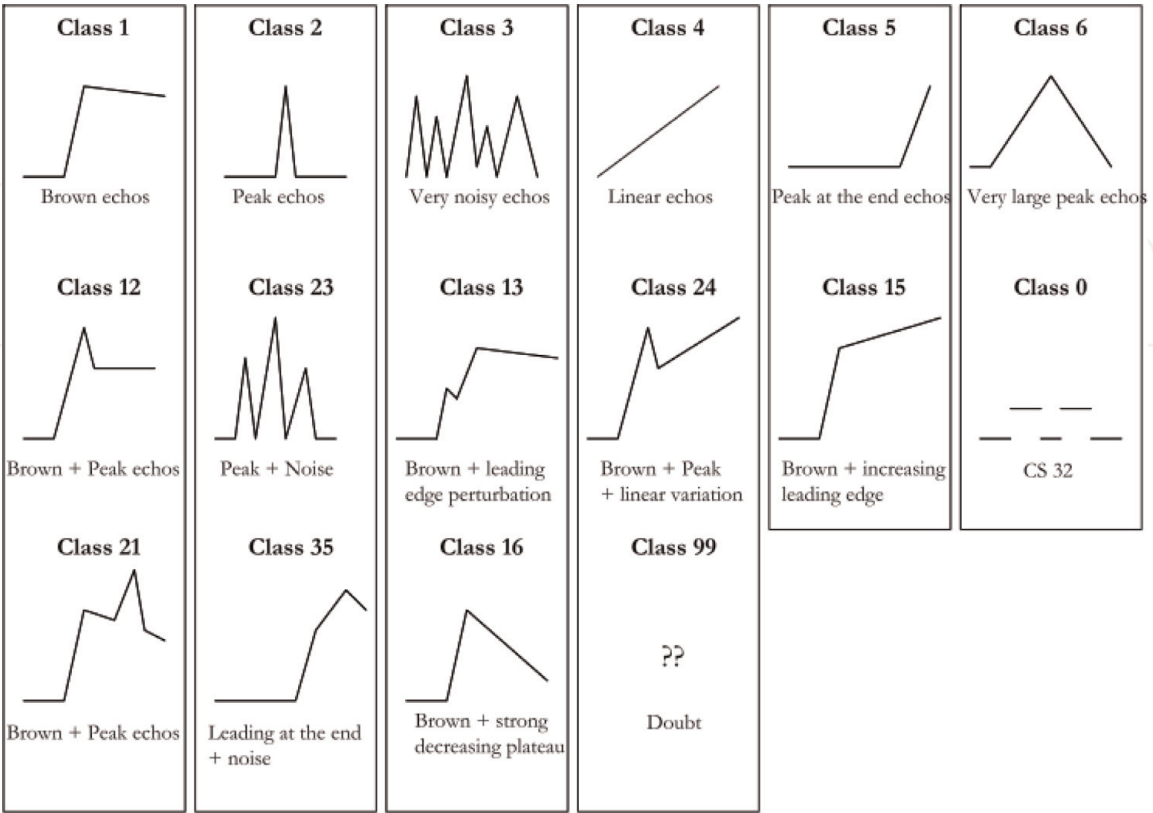


Figure 2.
Schematic representation of the waveform classes within the PISTACH processing [15].

Although the Brown [18] or Hayne [19] model is pretty successful over open ocean surface, there is little theoretic echo model elsewhere. Maybe the most universal coastal waveform model is the one proposed by Enjolras et al.:

$$P_r(t) = A \left[\iint_{S \in \text{water}} S_r \left(t - \frac{2h}{c} \right) \frac{G^2(\theta)}{h^4} \sigma_{\text{water}}(\theta) dS + \iint_{S \in \text{land}} S_r \left(t - \frac{2h}{c} \right) \frac{G^2(\theta)}{h^4} \sigma_{\text{land}}(\theta) dS \right] + P_0 \quad (1)$$

In the model the return power is expressed as the weighting average of the water surface echo and land surface echo. This model is not very practical: the geometry of the coastline, the relief, the nature of the terrain, etc., in a word, all characteristics of the coast that are extremely diverse all over the world. Therefore, it is difficult to determine the a priori parameters in the model.

There are also a couple of models, initially developed for ice surface, which are popularly used in coastal retracers, such as the so-called 5β model [20] and E model [21], with the following expressions:

$$P_r(t) = \beta_1 + \beta_2 \Phi \left(\frac{t - \beta_3}{\beta_4} \right) (1 + \beta_5 Q) \quad 5\beta \text{ model} \quad (2)$$

$$P_r(t) = \beta_1 + \beta_2 \Phi \left(\frac{t - \beta_3}{\beta_4} \right) \exp(-\beta_5 Q) \quad \text{E model} \quad (3)$$

where:

$$Q = \begin{cases} 0 & t < \beta_3 + \beta_4/2 \\ t - \beta_3 - \beta_4/2 & t > \beta_3 + \beta_4/2 \end{cases} \quad (4)$$

The two models are both reduced forms of Brown model, except permitting a negative mispointing angle. When $\beta_5 Q \ll 1$, the two models are essentially the same. The official Envisat ICE2 retracker is based on a simplified version of 5β model, where β_5 is always set to 0. Obviously, their physical mechanisms are based on open ocean surface and are often not suitable for coastal waveforms.

Hamili et al. [22] proposed a “Brown + Gaussian peaky (BGP)” model for the surface where a strong land scatter is presented in a Brown background. This model is suitable for the coastal zone with vertical structures behaving like corner reflectors.

As have been noted, the most cumbersome problem in coastal waveform is the contamination of land in the radar footprint. Fortunately, usually the contamination does not present in the entire waveform. One can retrack a portion of the waveform bins which are free from land contamination (this portion is called sub-waveform, e.g. [23–25]). After rejecting the contaminated bins one can still retrieve useful information.

In applying the sub-waveform technology, the most important issue is to determine the extent of a sub-waveform. The algorithms designed by PISTACH (RED3 and ICE3 [15]) define a sub-waveform with a fixed range: from the 22nd to the 52nd bins. Therefore no more than 1/3 of the 104 bins (for Jason-2) or 128 bins for (Envisat and HY-2A) are included in the retracker. Consequently, for the land-free waveforms, the precision is worse than the traditional retracers such as MLE3 and MLE4. ALES can be regarded as an improved version of RED3, in which the

sub-waveform extent is dependent on the significant wave height (SWH). As a consequence, under high sea state conditions, the sub-waveform can cover almost the entire waveform and is difficult to eliminate the contaminated bins.

In Xu et al. [26], a new strategy was proposed in which the extent of the sub-waveform was identified by the “differential spectrum”. For the Brown waveforms, the neighboring bins are unlikely to change rapidly except for the leading edge, so if there are land-contaminated bins, the corresponding differential spectrum will show a peaky pattern. The neighboring bins can thus be flagged as invalid ones in the retracking procedure. This strategy has been tested on HY-2A altimeter waveforms and has made significant improvement.

2.4.2.2 Model-free retrackers

The model-free retrackers (or empirical retrackers) do not assume a priori surface features. It can provide robust estimator regardless of physical background. The most famous model-free retracker is the OCOG (Offset Center Of Gravity) retracker that was proposed by Wingham et al. [27]. The idea is to approximate the waveform envelope to a rectangle shape, to find the center of gravity of the rectangle, and to subtract the half of the rectangle width (**Figure 3**) from the center of gravity:

$$t_{COG} = \frac{\sum_{i=1}^N i V_i^2}{\sum_{i=1}^N V_i^2} A = \sqrt{\frac{\sum_{i=1}^N V_i^4}{\sum_{i=1}^N V_i^2}} W = \frac{\left[\sum_{i=1}^N V_i^2\right]^2}{\sum_{i=1}^N V_i^4} t_0 = t_{COG} - W/2 \quad (5)$$

Another retracker is the simple threshold retracker. Finding the bin with the maximum power, say, M , and finding the first bin whose power exceeds $M^*p\%$, where $p\%$ is a threshold percentage.

OCOG retracker is the most robust retracker, but it has been shown that OCOG retracker usually has relatively large bias (even larger than the simple threshold retracker). On the other hand, the threshold retracker can generate unexplainable results occasionally. The modified threshold retracker adopts the advantages of both retrackers. It uses A in Eq. (5) rather than M as the maximum bin power. The modified threshold retracker is the most widely used model-free retracker. The official Envisat ICE1 retracker and PISTACH ICE1 and ICE3 retrackers all belong to modified threshold retrackers.

Although it is pretty easy to implement, the most troublesome issue of the (modified) threshold retracker is to determine the value of $p\%$. Apparently 50% is reasonable, but various studies gave different values. Tseng et al. [29] pointed that

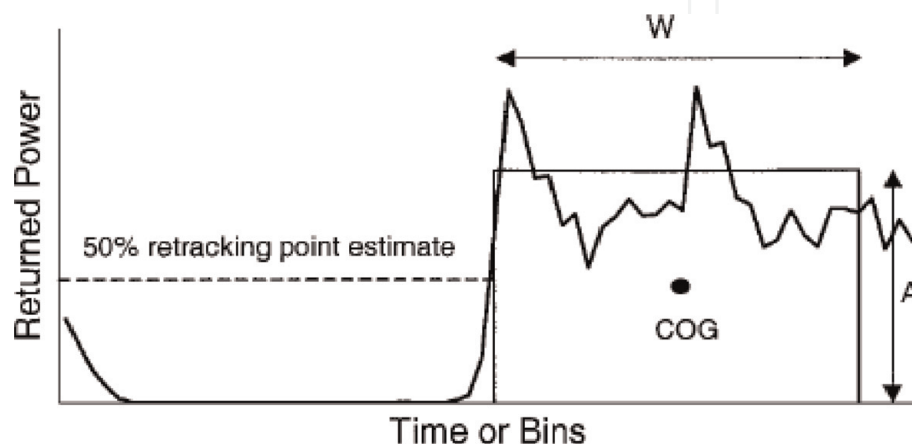


Figure 3.
 Principle of an OCOG algorithm (from [28]).

20% is better, and the PISTACH ICE retrackers preferred $p = 30\%$ [15]. It seems that the threshold somewhat depends on the characteristics of the study area.

Another model-free algorithm is the curve spline interpolation. It has been mentioned briefly by a couple of authors without details. The idea is to interpolate between neighboring bins when implementing the threshold retracker. It can unlikely bring significant difference from the threshold retracker.

2.4.2.3 Retracking strategy

Scientists have been debating for many years on the retracking strategy. Some-one insisted that applying one single algorithm for all kinds of waveforms is a better choice. For instance, ALES developers use their retracker even over open ocean surface, and their analysis shows that the precision of ALES is not substantially worse than the official MLE4 over open ocean surface. On the other hand, PISTACH carried out a waveform classification before retracking. The classification is primarily dependent on the waveform pattern and secondarily on auxiliary information such as land cover model. Different retrackers are implemented for different waveform classes.

Our opinion is that a classification may be preferable because the waveforms have a large variety. A specialized algorithm for a certain waveform would improve the retracker precision significantly. There may be bias between different retrackers and inconsistency in the retracker transition. If the bias between retrackers is not compensated, there might be unexplained jumps in the sea level measurements, and this is the reason why some researchers are inclined to use one unique retracker. We hold that this problem can be solved either by simulative analysis or by calibration.

2.5 Geophysical corrections at the coast

The geophysical corrections near the coast also need specific considerations. Many terms of the geophysical corrections have larger uncertainty at the coast than over the open ocean.

2.5.1 Atmospheric propagation corrections

The most uncertain error source comes from the wet tropospheric correction because the onboard radiometer suffers severely from land contamination in the coastal area. A simple but effective approach is to extrapolate a model-based correction (using, for example, atmospheric reanalysis data from the European Center for Medium-Range Weather Forecasts, ECMWF), but the corresponding spatial resolution is relatively low for coastal applications. Other approaches include an improved radiometer-based correction accounting for the land contamination effect [30], or the computation of GNSS-derived Path Delay (GPD, Fernandes et al. [31]).

Concerning the ionospheric correction, the imperfect coastal altimeter range measurements lead to significant errors, generating outliers in the correction values. The median + MAD (mean absolute bias) criterion is more preferable than the mean + standard deviation criterion, because the outliers are easier to detect and remove. The along-track profile of ionospheric corrections is further spatially low-pass filtered with a cutoff frequency of 100 km.

2.5.2 Sea state bias

Another important correction is the sea state bias (SSB). The SSB depends on the retracking algorithm, because it contains the tracker bias. A careful analysis showed

that for Jason-2 GDR products, the SLAs obtained from MLE3 and MLE4 retrackers have large bias. From a statistical analysis using cycles 1–238 for a couple of altimeter passes over the open ocean, we obtained: $SLA_{MLE3} - SLA_{MLE4} = +2.3$ cm. Near the coast, this bias appeared to be even larger and even more critical as it is not constant. **Figure 4** shows both MLE3 and MLE4 SSB corrections as a function of SWH for an arbitrary pass (cycle 16, pass #153). MLE3 SSB has a clear bias ($\sim +3$ cm) relative to MLE4 SSB. Moreover, MLE3 SSB seems to have more outliers, in particular near the coast. The bias observed between MLE3 and MLE4 sea level estimates mainly corresponds to a bias in the SSB corrections.

Deeper investigation showed that the MLE3 SSB outliers are often related to large altimeter waveform-derived off-nadir angle estimation values [32], which probably suffer from errors given the good attitude control of Jason-2 satellite. For this reason, we adopted the MLE4 SSB in the computation of all SLAs, resulting in a relative bias <1 cm for all retrackers.

2.5.3 Ocean tide and DAC

The coastal ocean tide corrections, provided by global models, are also far from accurate. There are two families of tide solutions in most altimetry products: the family of the Goddard Ocean Tide (GOT) models developed by Ray et al. [33], and the family of the Finite Element Solution (FES) models developed by Lyard et al. [34].

Ray compared different tide solutions against 196 shelf-water tide gauges and 56 coastal tide gauges. Their accuracy was characterized by the RSS (root sum square) error of the eight main tidal constituents (Q1, O1, P1, K1, N2, M2, S2, and K2). For the shelf-water gauges, the accuracy of GOT4.8 was 7.04 cm (European coasts) or 6.11 cm (elsewhere), while the accuracy of FES2012 was 4.82 cm (European coasts) or 4.96 cm (elsewhere). For the coastal tide gauges, the accuracy of GOT4.8 and FES2012 was 8.46 and 7.50 cm, respectively [35]. In comparison, the accuracy of GOT4.7 and FES2004 in shelf-water was 7.77 and 10.15 cm, respectively. These results illustrate the significant improvement in coastal ocean tide solution during the last decade.

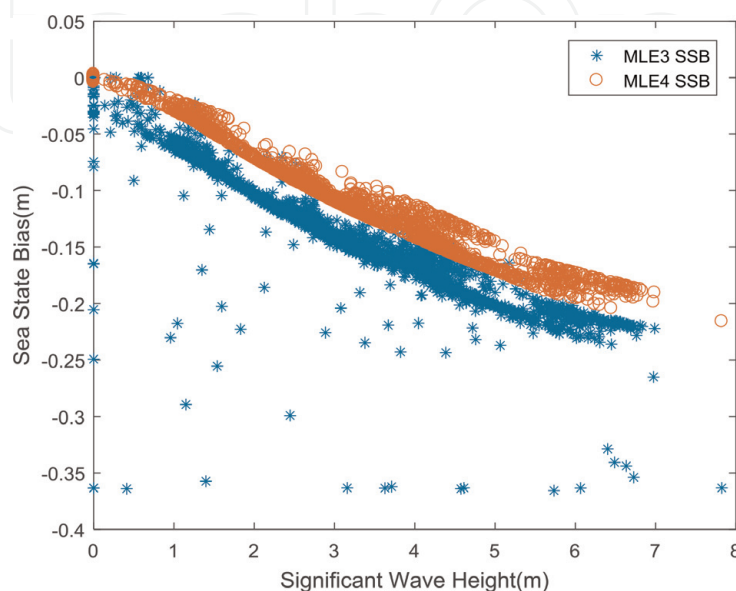


Figure 4.
 SSB difference with respect to the significant wave height (SWH).

3. Case study offshore Hong Kong

In this section, Hong Kong coastal zone is chosen as an example to demonstrate the methodology and potential of the coastal altimetry technology. We focus on Jason-2 data here, and other altimetry missions like HY-2 can also be assimilated to achieve denser coverage and cross validation. To exploit the potential of the current endeavors in coastal altimetry, the three products aforementioned are merged and evaluated.

3.1 Study area

Hong Kong (HK) is located just south of the Tropic of Cancer. The climate displays clear seasonal variations. The southwesterly/northeasterly monsoon results in warm wet summers and cool dry winters. HK also frequently suffers from typhoons. On the western side of the HK island flows the Zhujiang River (Pearl River), which brings abundant freshwater, giving rise to a high salinity (hence, sea water density) gradient. All these factors impact significantly on the regional sea level variations.

The HK coast has an extremely complex geomorphology. As shown in **Figure 5**, many tiny islands lie within the altimeter footprints. Therefore, the corresponding altimeter and radiometer measurements are severely contaminated by land effects. This makes this area particularly relevant for analyzing the performances of coastal altimetry data.

The HK coastal topography is more than irregular. Despite a narrow band between 21.8°N and 22°N , where the depth is steeply falling down to ~ -60 m, the study area has very shallow waters. We can thus expect complex local tides and currents, which can influence sea level variations.

3.2 Data sets

3.2.1 Jason-2 altimetry products

The time span in this study covers 6.5 years: from July 2008 to December 2014. The coastal Jason-2 products analyzed in this study are X-TRACK, ALES, and PISTACH.

The retracers available in the different L2 products are summarized in **Table 2**. The standard GDRs include two solutions: MLE3 and MLE4. The mechanisms of these two retracers are similar: fitting the waveform to a Brown model [18] based on the MLE (essentially, nonlinear least squares) techniques. MLE3 estimates three parameters: epoch (i.e., altimetric range), significant wave height (SWH), and amplitude (i.e., backscatter coefficient), while MLE4 also retrieves the square of off-nadir angle. The PISTACH products provide four retracers: OCE3, RED3, ICE1, and ICE3 [15]. OCE3 is essentially the same as the MLE3. ICE1 is a modified threshold retracker. RED3 and ICE3 are the sub-waveform counterparts of OCE3 and ICE1, respectively. ALES is an improved version of RED3, in which the sub-waveform length can vary from 39 bins (for $\text{SWH} = 1$ m) to 104 bins (i.e., the entire waveform, for $\text{SWH} \geq 17$ m).

In PISTACH and X-TRACK, state-of-the-art geophysical corrections other than those of the official GDR are provided. For X-TRACK, the ocean tide solution and the DAC are provided individually, while in PISTACH, two to three values are given for each correction. Different sets of correction terms obviously lead to different coastal sea level estimates.

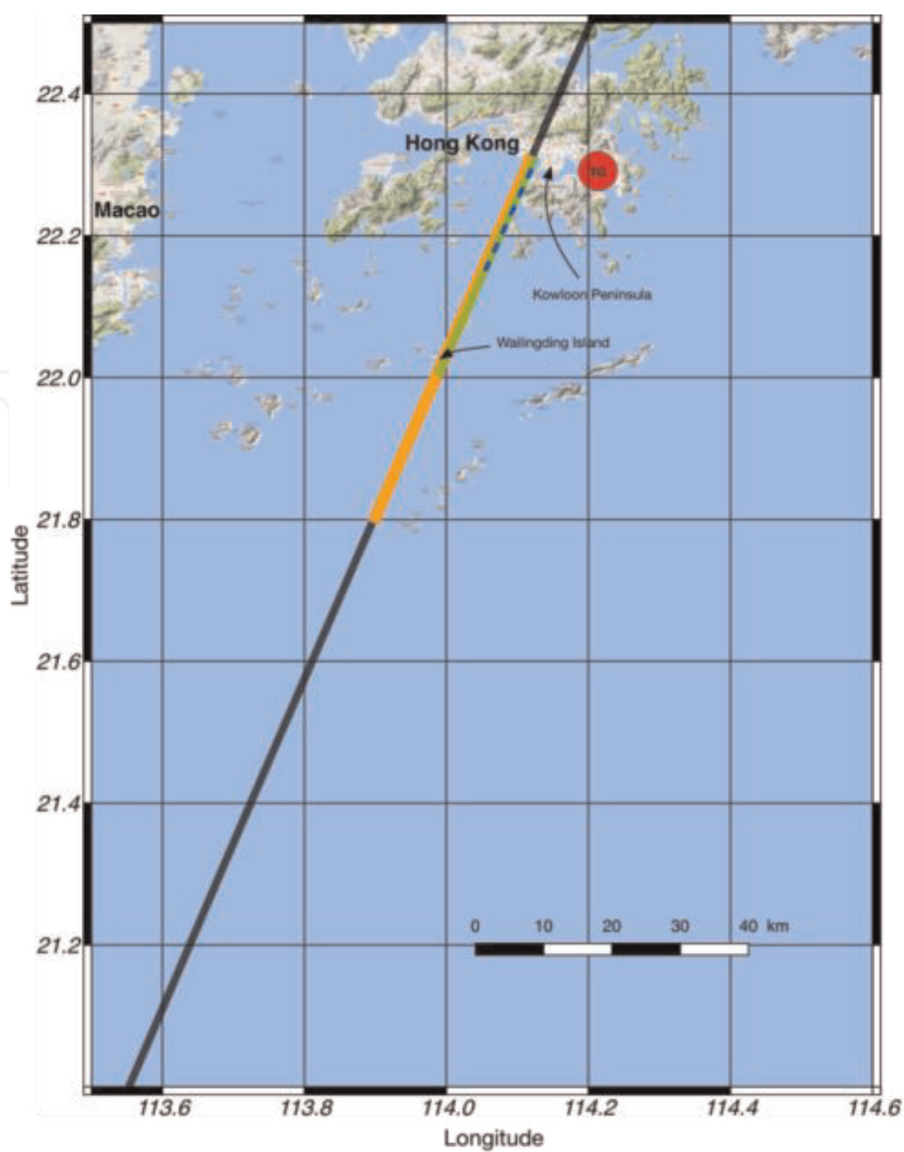


Figure 5. Map showing the study area, the selected Jason-2 pass 153 (black and colored line) and the Quarry Bay tide gauge (red circle) located ~10 km away from the Jason-2 pass.

Retracker	Product	Idea	Sub-waveform	Comments
MLE4	(S)GDR	Brown model	No	Official standard retracker.
MLE3	(S)GDR	Brown model	No	
OCE3	PISTACH	Brown model	No	Same as MLE3
RED3	PISTACH	Brown model	Fixed: bins: $t_0 + [-10:20]$	Simplified version of ALES
ALES	ALES	Brown model	Adaptive to the SWH	Two-pass retracker
ICE1	PISTACH	Modified threshold	No	
ICE3	PISTACH	Modified threshold	Fixed: bins: $t_0 + [-10:20]$	

Table 2. Overview of different retrackers applied in different altimetry products.

3.2.2 Tide gauge data

The Quarry Bay tide gauge (located at 114.22°E, 22.28°N) regularly measures sea level with an accuracy of ≤ 1 cm and is well calibrated every other year [36]. The

tide gauge lies near the northern coast of the HK Island, separated from the Kowloon Peninsula by the Victoria Harbor (see **Figure 5**), where $\sim 95\%$ of the shoreline is shaped by human activity [37]. Thus, sea level on this area is expected to be intensively influenced by anthropogenic activities. Hourly tide gauge data are archived and distributed by the Sea Level Center of the University of Hawaii (<https://uhslc.soest.hawaii.edu>).

A harmonic analysis was first applied to the tide gauge data in order to remove the tidal signals from the sea level time series. A bias (defined as the time-averaged sea level value) was also removed to make the sea level anomaly (SLA) consistent with the altimetry data. Finally, the hourly tide gauge data were interpolated to the Jason-2 satellite overhead time. The tide gauge-based sea level time series interpolated to the closest Jason-2 observations is shown in **Figure 6**. A large seasonal cycle due to the monsoon can be observed, modulated by high-frequency variations up to several tens of cm. A peak in the tide gauge sea level time series can be noticed at cycle 228. It is caused by a storm surge associated with the Typhoon Kalmaegi that angrily attacked on the HK coast before sunrise on 16 September 2014. The Jason-2 altimeter flew over the HK area at 3:45 am (local time) on that day, and the peak captured the typhoon event. Although it would be quite valuable for the storm surge investigation, in our analysis this peak was eliminated as an outlier.

3.3 Methodology

3.3.1 Altimetry data processing

As indicated above, current coastal altimetry products differ in terms of content. Therefore, in the beginning of the processing the different data sets were merged to obtain homogeneous variables for further comparison. Because there is no waveform data in PISTACH, we used the waveforms provided in ALES and merged PISTACH and ALES using the measurement time common to all products. We also projected all the along-track, cycle-by-cycle L2 data onto the X-TRACK 1-Hz reference grids to benefit from the X-TRACK improved corrections.

Once all the propagation and geophysical corrections are removed, the sea surface height (SSH, i.e., the sea level referred to a reference ellipsoid) can be deduced from the altimeter range. If we further remove a mean sea surface in order to

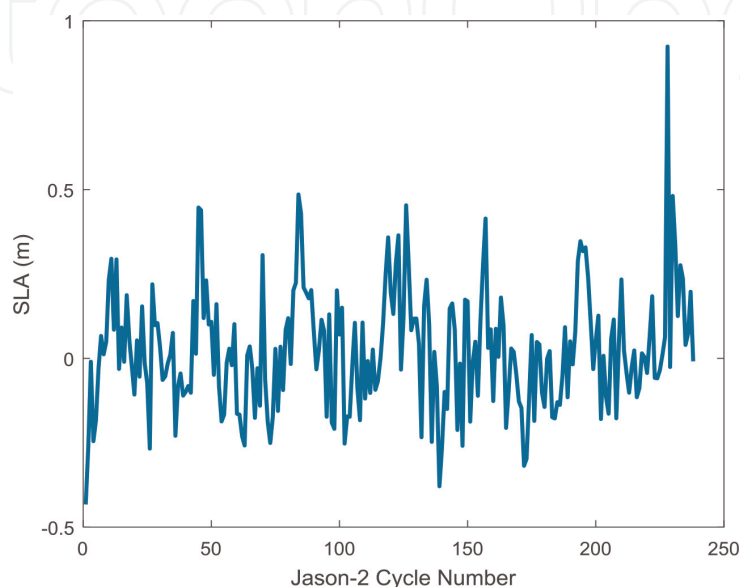


Figure 6.
HK tide gauge sea level time series (in meters) interpolated to Jason-2 observations.

eliminate the influence of the geoid undulation, the sea level anomaly (SLA) can be obtained. In this study, we use SLA data, computed as follows:

$$SLA = H - R - \Delta R_{iono} - \Delta R_{dry} - \Delta R_{wet} - \Delta R_{ssb} - \Delta R_{tide} - \Delta R_{DAC} - MSS \quad (6)$$

In Eq. (6), H is the satellite height, R is the altimeter range, ΔR_{iono} , ΔR_{dry} , and ΔR_{wet} are the ionospheric, dry, and wet tropospheric corrections, respectively, ΔR_{ssb} is the sea state bias, ΔR_{tide} is the tide correction (sum of the ocean tide, pole tide, and solid Earth tide), ΔR_{DAC} is the dynamic atmospheric correction, and MSS is mean sea surface.

At the coast, R is often not directly available, so it can be derived as follows:

$$R = T + E \times (c/2) + D + M + 0.180 \quad (7)$$

where T is the onboard tracking range, E is the retracked offset (with time dimension), " $c/2$ (c being the light velocity)" is the scaling factor from time to range, D is the Doppler correction, M is the instrument imperfection bias [38, 39], and 0.180 is a bias (in meters) due to wrong altimeter antenna reference point [40].

In this study, SLA time series are computed using the altimeter ranges by six retrackers: ALES, MLE3, MLE4, RED3, ICE1, and ICE3. Eq. (7) was used to compute R in the first step, and then Eq. (6) was applied to derive the SLA. To validate our calculation method, we compared our MLE4 SLA with the equivalent official "ssha" parameter in the GDRs and found a very good consistency.

3.3.2 Sea level data analysis

After generating the SLA time series, useful oceanography information can be retrieved. Because of the presence of monsoon, the annual and semi-annual signals are both significant near the HK coast. Therefore, to the first order, SLA variations can be modeled as follows:

$$SLA(t) = a_1 \cos(2\pi t/T_{year}) + a_2 \sin(2\pi t/T_{year}) + a_3 \cos(4\pi t/T_{year}) + a_4 \sin(4\pi t/T_{year}) + a_5 t + a_6 + \varepsilon(t) \quad (8)$$

where $T_{year} = 365.2425$ days, $\varepsilon(t)$ is the residual SLA, and a_1 to a_6 are the regression coefficients to be estimated. The estimation uncertainty of the coefficients can be determined from the square root of the diagonal elements in the covariance matrix of the coefficient vector. The linear trend can be inferred from a_5 annual/semi-annual amplitude, and phase can be deduced from a_1 to a_4 :

$$A_{annual} = \sqrt{a_1^2 + a_2^2}; A_{semi-annual} = \sqrt{a_3^2 + a_4^2} \quad (9)$$

$$\Phi_{annual} = \arctan(a_2/a_1); \Phi_{semi-annual} = \arctan(a_4/a_3) \quad (10)$$

3.4 Results

Some results are reported here, in which the sea level for a certain cycle is the average of all the valid measurements within ≤ 10 distance from the coast. Interested readers can refer to [41] for more details.

3.4.1 Solutions derived from the different Retrackers

For each retracker, we computed a spatially averaged 20-Hz SLA time series as well as the associated 20-Hz noise level (defined as the standard deviation of

the 20-Hz SLA series). ALES solution provides the lowest noise level after editing, and MLE4 is slightly less noisy than MLE3. Concerning the three experimental retrackerers used in PISTACH, ICE3 has the lowest noise level, and RED3 is slightly less noisy than ICE1.

Sea level trends of are summarized in **Table 3** (except for OCE3 in PISTACH, which is the same as MLE3). As a reference, after correcting for VLM, we find a trend of $+5.5 \pm 2.0$ mm/yr. at the tide gauge site.

MLE3 and ALES trends are both close to the tide gauge trend (within 0.5 mm/yr). The trends estimated from MLE4 are slightly lower than for ALES and MLE3 but the difference is within the error bar. The trends deduced from the PISTACH retrackerers disagree significantly with the tide gauge trend: both ICE3 and RED3 show unrealistic large values ($>+5$ cm/yr), while ICE1 shows a negative trend of -2 cm/yr. The ICE1 retracker may be inherently not accurate enough to derive trends, but ICE3 and RED3 data surprisingly display large jumps of about $+20$ cm. This would severely influence the corresponding sea level trend estimates. In the remaining part of the study, we concentrate on MLE3, MLE4, and ALES which, in the context of our study, appear to be the best available retrackerers for Jason altimetry.

3.4.2 Coastal seasonal signal along the Jason-2 pass

The amplitude and phase of the seasonal signal are also computed for all sea level time series. The results are shown in **Table 4**. The altimetry annual phases lie around 340° and are significantly larger than the tide gauge-based phase. Amplitudes are also slightly larger. The semiannual phases lie around 240° and are very close to the tide gauge-based phase. Amplitudes are slightly smaller. We cannot exclude the possibility that there is some local seasonal signal at the tide gauge site.

3.4.3 Relative performances of MLE4, MLE3, and ALES near Hong Kong

The sea level residuals obtained after removing the trend and seasonal signal are shown in **Figure 7** for MLE3, MLE4, ALES, and the tide gauge data. A 3-month low pass filter was applied to the different SLA time series to reduce the intrinsic 59-day erroneous signal discovered in Jason altimetry missions [42, 43]. The standard deviations of the altimetry SLA residuals with respect to the tide gauge residuals,

Retracker	ALES	MLE3	MLE4	ICE1	ICE3	RED3
Linear trend and uncertainty (mm/yr)	$+5.9 \pm 1.5$	$+5.0 \pm 1.6$	$+4.2 \pm 1.6$	-29.1 ± 2.4	$+57.5 \pm 2.3$	$+55.3 \pm 2.1$

Table 3.
Estimated linear trend and associated uncertainty (mm/yr) as a function of sea level data source and case.

Data source	Annual	Semiannual
ALES	13.05/344	6.03/235
MLE3	13.29/338	6.17/241
MLE4	12.96/339	6.02/236
Tide gauge	11.46/311	7.62/236

Table 4.
Estimated annual/semiannual amplitude (cm) and phase (degree) as a function of sea level data source and case.

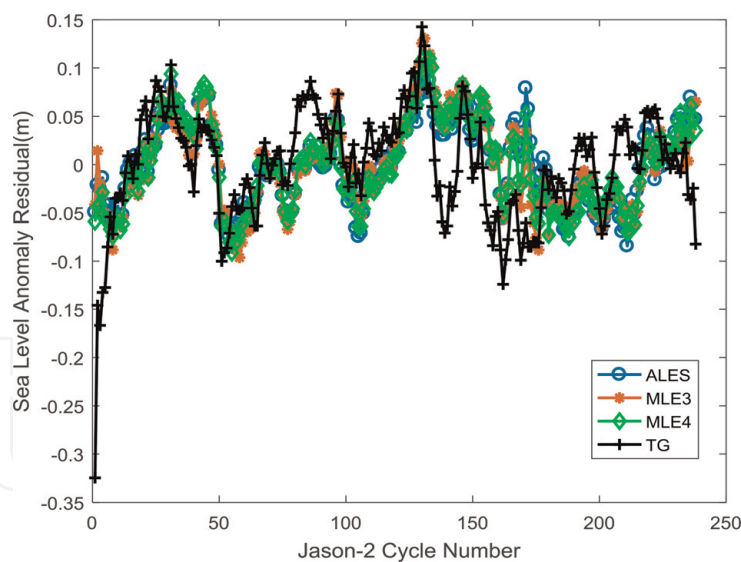


Figure 7.
Detrended and deseasoned SLA time series based on ALES, MLE3, and MLE4, with 3-month smoothing (tide gauge SLA—Noted TG—Is shown as reference).

SLA series	ALES	MLE3	MLE4
Agreement	5.12	4.82	4.88

Table 5.
Deseasoned and detrended SLA standard deviation w.r.t. tide gauge sea level (cm).

before and after the 3-month smoothing, are given in **Table 5**. The improvement due to the smoothing is significant, the standard deviations decreasing by more than 50%. The consistency between the altimetry and tide gauge residuals is about 5 cm, which is encouraging given that the study area is quite complex. ALES SLA has a slightly larger standard deviation with respect to tide gauge sea level.

4. Conclusions and prospective

In this paper, a promising technology: coastal altimetry is described in many facets. The advances in the last decade are reviewed, especially on the coastal waveform processing. In the Hong Kong offshore case study, we find that the coastal sea level trend is about twice as much as the one observed further offshore (which can be inferred as +2.7 mm/yr. from the ESA Sl_CCI product [41]). It suggests that in the Hong Kong region, the short-term sea level trend significantly increases when approaching the coast. Scientists worldwide have discovered many new features in different coastal regions (e.g., the Mediterranean coast, the Australia coasts, the coasts of the United States, West African coast, etc. [44]), and the technology would be further exploited in the future benefiting from the new conceptual altimeters.

Delay Doppler Altimeter (DDA), or Synthetic Aperture Radar (SAR) altimeter, is one of the most exciting advances in altimetry [45]. The along-track resolution is significantly improved by an order magnitude (from several kilometers to a few hundred meters), which is particularly useful to capture the small scale features. Cryosat-2 is the first satellite to demonstrate the DDA approach, and Sentinel-3 satellites operate in DDA mode all the time [46, 47]. China and other countries are also planning to launch altimeters of this type. A few investigations have been

reported to show the potential of the DDA technology, and solid contribution would be made to the coastal community if more dedicated waveform processing and geographic corrections approaches are developed and validated.

Acknowledgements

This study is supported by the National Natural Science Foundation of China (Grant No. 41876209) and by the State Key Laboratory of Tropical Oceanography, South China Sea Institute of Oceanology, Chinese Academy of Sciences (Project No. LTO 1908). Much of the work reported in this chapter is the outcome of Xi-Yu Xu during his visit in Laboratoire d'Études en Géophysique et Océanographie Spatiales (LEGOS), Observatoire Midi-Pyrénées, France. Anny Cazenave and Florence Birol, the collaborators of Xi-Yu Xu in Legos, are gratefully acknowledged for their substantial help and insightful advice.

Author details


Xi-Yu Xu^{1*}, Ke Xu¹, Ying Xu² and Ling-Wei Shi¹

1 The Key Laboratory of Microwave Remote Sensing, National Space Science Center, Chinese Academy of Sciences, Beijing, China

2 National Satellite Ocean Application Service, Beijing, China

*Address all correspondence to: xuxiyu@mirslab.cn

IntechOpen

© 2019 The Author(s). Licensee IntechOpen. This chapter is distributed under the terms of the Creative Commons Attribution License (<http://creativecommons.org/licenses/by/3.0>), which permits unrestricted use, distribution, and reproduction in any medium, provided the original work is properly cited. 

References

- [1] Vignudelli S, Kostianoy AG, Cipollini P, Enveniste J, editors. *Coastal Altimetry*. Berlin Heidelberg: Springer-Verlag; 2011. 576p
- [2] Fu LL, Cazenave A, editors. *Satellite Altimetry and Earth Science. International Geophysics Series. Vol. 69*. San Diego: Academic Press; 2000. 463p
- [3] Stammer D, Cazenave A, editors. *Satellite Altimetry over Oceans and Land Surfaces*. CRC Press; 2017. ISBN: 978-1-4987-4345
- [4] Kaula W, editors. NASA (Williamstown report): *The Terrestrial Environment, Solid-Earth and Ocean Physics, Application of Space and Astronomic Techniques. Report of a Study at Williamstown, MA, NASA*; 1969
- [5] Fu L, Christensen E, Yamarone C, et al. TOPEX/POSEIDON mission overview. *Journal of Geophysical Research*. 1994;**99**:24369-24381
- [6] Menard Y, Fu LL, Escudier P, et al. The Jason-1 mission. *Marine Geodesy*. 2003;**26**:131-146
- [7] Lambin J, Rosemary M, Fu LL, et al. The Jason-2 / OSTM mission. *Marine Geodesy*. 2010;**33**:4-25
- [8] Dumont JP, et al. *Jason-3 Products Handbook*. CNES: SALP-MU-M-OP-16118-CN; 2017
- [9] Benveniste J. Towards more efficient use of radar altimeter data. *ESA Bulletin*. 1993;**76**
- [10] Benveniste J, Roca M, Levrini G, et al. The radar altimetry mission: RA-2, MWR, DORIS, and LRR. *ESA Bulletin*. 2001;**106**:67
- [11] Verron J, Sengenès P, Lambin J, et al. The SARAL/AltiKa altimetry satellite mission. *Marine Geodesy*. 2015;**38**:2-21
- [12] Xu K, Jiang JS, Liu HG. HY-2A radar altimeter design and in flight preliminary results. In: *Proceedings of the IEEE International Geoscience and Remote Sensing Symposium*. Melbourne; 2013. pp. 1642-1644
- [13] Birol F, Fuller N, Lyard F, Cancet M, Niño F, Delebecque C, et al. Coastal applications from nadir altimetry: Example of the X-TRACK regional products. *Advances in Space Research*. 2017;**59**:936-953. DOI: 10.1016/j.asr.2016.11.005
- [14] Passaro M, Cipollini P, Vignudelli S, Quartly GD, Snaith HM. ALES: A multimission adaptive subwaveform retracker for coastal and open ocean altimetry. *Remote Sensing of Environment*. 2014;**145**:173-189
- [15] Mercier F, Rosmorduc V, Carrere L, Thibaut P. *Coastal and Hydrology Altimetry Product (PISTACH) Handbook*; CLS-DOS-NT-10-246. Paris, France: CNES; 2010
- [16] Berry PAM, Jasper A. *Retracking ERS-1 Land Altimeter Data Using an Expert System*. Southampton: U.K. Geophysical Assembly; 1997
- [17] Schwatke C, Dettmering D. Mission-independent classification of altimeter waveforms for applications in the Open Ocean, at the coastal zone and over land. In: *10th Coastal Altimetry Workshop*. Florence; 2017
- [18] Brown G. The average impulse response of a rough surface and its applications. *IEEE Transactions on Antennas and Propagation*. 1977;**25**: 67-74
- [19] Hayne GS. Radar altimeter mean return waveforms from near-normal–

- incidence ocean surface scattering. IEEE Transactions on Antennas and Propagation. 1980;28(5):687-692
- [20] Martin TV, Zwally HJ, Brenner AC, Bindschadler RA. Analysis and Retracking of continental ice sheet radar altimeter waveforms. Journal of Geophysical Research. 1983;88: 1608-1616
- [21] Anzenhofer M, Shum CK, Rentsch M. Coastal Altimetry and Applications. Ohio State University Geodetic Science and Surveying Technical Report No. 464; 1999. 36p
- [22] Halimi A, Mailhes C, Tourneret J-Y, Thibaut P, Boy F. Parameter estimation for peaky altimetric waveforms. IEEE Transactions on Geoscience and Remote Sensing. 2013;51(3):1568-1577
- [23] Hwang C, Guo J, Deng X, Hsu H-Y, Liu Y. Coastal gravity anomalies from retracked Geosat/GM altimetry: Improvement, limitation and the role of airborne gravity data. Journal of Geodesy. 2006;80:204-216
- [24] Bao LF, Lu Y, Wang Y. Improved retracking algorithm for oceanic altimeter waveforms. Progress in Natural Science. 2009;19:195-203. DOI: 10.1016/j.pnsc.2008.06.017
- [25] Yang L, Lin MS, Liu Q, Pan DL. A coastal altimetry retracking strategy based on waveform classification and subwaveform extraction. International Journal of Remote Sensing. 2012;33: 7806-7819
- [26] Xu XY, Xu K, Birol F, Yang SB. HY-2A satellite altimetry advanced waveform processing offshore Hong Kong. In: Proceedings of the IEEE International Geoscience and Remote Sensing Symposium. Valencia; 2018. pp. 7668-7671
- [27] Wingham DJ, Rapley CG, Griffiths H. New techniques in satellite tracking systems. In: Proceedings of the IEEE International Geoscience and Remote Sensing Symposium; 1986. pp. 1339-1344
- [28] Deng X, Featherstone WE, Hwang C, Berry PAM. Estimation of contamination of ERS-2 and POSEIDON satellite radar altimetry close to the coasts of Australia. Marine Geodesy. 2002;25:249-271
- [29] Tseng KH, Shum CK, Yi Y, et al. The improved retrieval of coastal sea surface heights by retracking modified radar altimetry waveforms. IEEE Transactions on Geoscience and Remote Sensing. 2014;52(2):991-1001
- [30] Brown S. A novel near-land radiometer wet path-delay retrieval algorithm: Application to the Jason-2/OSTM advanced microwave radiometer. IEEE Transactions on Geoscience and Remote Sensing. 2010; 48:1986-1992
- [31] Fernandes MJ, Lázaro C, Ablain M, Pires N. Improved wet path delays for all ESA and reference altimetric missions. Remote Sensing of Environment. 2015;169:50-74. DOI: 10.1016/j.rse.2015.07.023
- [32] He-Guang L, Xi-Yu X, Le Y. Analysis of the dependence on retrackers of the Jason satellites altimetry products. In: Proceedings of the IEEE International Geoscience and Remote Sensing Symposium. Valencia; 2018. pp. 7672-7675
- [33] Ray RD, Egbert GD, Erofeeva SY. Tide predictions in shelf and coastal waters: Status and prospects. In: Vignudelli S, Kostianoy AG, Cipollini P, Benveniste J, editors. Coastal Altimetry. Berlin: Springer; 2011. Chapter 7
- [34] Lyard F, Lefevre F, Letellier T, Francis O. Modelling the global ocean tides: Modern insights from FES2004. Ocean Dynamics. 2006;56:394-415

- [35] Ray R. Status of modeling shallow-water ocean tides: Report from Stammer international model comparison project. In: Proceedings of the NASA/CNES Surface Water and Ocean Topography (SWOT) Science Definition Team (SDT) Meeting; 26–28 June 2014; Toulouse, France; 2014
- [36] Chan YW. Tide reporting and applications in Hong Kong, China. 2006. Available from: www.glosssealevel.org/publications/documents/hong_kong_2006.pdf
- [37] Lai WS, Matthew JP, Ho KY, et al. Hong Kong's marine environments: History, challenges and opportunities. *Regional Studies in Marine Science*. 2016;**8**:259-273
- [38] Thibaut P, Amarouche L, Zanife LOZ, Stunou N, Vincent P, Raizonville P. Jason-1 altimeter ground processing look-up correction tables. *Marine Geodesy*. 2004;**27**:409-431
- [39] Xu XY, Xu K, Wang ZZ, Liu HG, Wang L. Compensating the PTR and LPF features of the HY-2A satellite altimeter utilizing look-up tables. *IEEE Journal of Selected Topics in Applied Earth Observations and Remote Sensing*. 2015;**8**:149-159
- [40] Dumont JP, Rosmorduc V, Carrere L, et al. OSTM/Jason-2 Products Handbook (Issue: 1 rev 11); SALP-MU-M-OP-15815-CN; 2017
- [41] Xu XY, Birol F, Cazenave A. Evaluation of coastal sea level offshore Hong Kong from Jason-2 altimetry. *Remote Sensing*. 2018;**10**(2):282
- [42] Masters D, Nerem RS, Choe C, et al. Comparison of global mean sea level time series from TOPEX/Poseidon, Jason-1, and Jason-2. *Marine Geodesy*. 2012;**35**:20-41
- [43] Chambers DP, Cazenave A, Champollion N, et al. Evaluation of the global mean sea level budget between 1993 and 2014. *Surveys in Geophysics*. 2017;**38**:309-327
- [44] Ablain M, Legeais JF, Prandi P, Marcos M, Fenoglio-Marc L, Dieng HB, et al. Satellite altimetry-based sea level at global and regional scales. *Surveys in Geophysics*. 2017;**38**:7-31
- [45] Raney RK. The delay/Doppler radar altimeter. *IEEE Transactions on Geoscience and Remote Sensing*. 1998;**36**(5):1578-1588
- [46] Wingham D, Francis CR, Baker S, et al. CryoSat: A mission to determine the fluctuations in Earth's land and marine ice fields. *Advances in Space Research*. 2006;**37**(4):841-871
- [47] Donlon C, Berruti B, Frerick J, et al. The sentinel-3 mission overview. In: Proceedings of the 2011 EUMETSAT Meteorological Satellite Conference; 5–9 September; Oslo, Norway; 2011